NUMERICAL MODELLING OF ARCHED STRUCTURES

I. BASILIO[1], D.V. OLIVEIRA[2], P.B. LOURENÇO[3] AND L.F. RAMOS[2]

[1]PhD Student, [2]Assistant Professor, [3]Full Professor
School of Engineering, Department of Civil Engineering
University of Minho, Guimarães, Portugal

SUMMARY

Curved shapes represent an interesting and aesthetical constructive solution. Nevertheless, as for any structural element, a clear knowledge about its properties and behaviour is needed. Aiming at tackling such challenge and given the importance that structural retrofitting represents nowadays, a study about the modelling of masonry arched structures strengthened with FRP is presented in this paper. Final concluding remarks and results discussion are given regarding comparison between experimental and the numerical model constructed to reproduce the laboratory tests.

INTRODUCTION

A growing interest in the preservation of historic structures has created a need of methods for the analysis of load-bearing masonry structures, such as arches and vaults. Vaults are one of the most common structural shapes present in the architectural heritage of the world. These structures are defined as structures in which the load bearing is clearly associated with the distribution of material in space. Among the materials used to repair or upgrade ancient masonry structures, there has been an increasing interest devoted to the use of FRP (fiber-reinforced polymer) composites in the form of bonded surface reinforcements, which are being more and more used.

In order to evaluate the behaviour of brick masonry arches strengthened with FRP, a combined experimental-numerical research project was carried out at Universidade do Minho. The experimental program consisted partially in the testing of twelve scaled semicircular brick masonry arches, plain and strengthened with GFRP composites. All arch specimens were constructed at scale 1:2 in order to optimize expenses related to raw materials and workmanship as well as to achieve a quicker construction process and a feasible testing setup. For further details see Basilio (2007). In this paper, the numerical analysis of the unstrengthened and strengthened masonry arches is presented, in order to evaluate the effectiveness of different GFRP strengthening strategies. The nonlinear behaviour of the materials was considered in the analysis.

STRUCTURAL MODEL FOR MASONRY ARCHES

The approach followed here concerning modelling was based on the micro-modelling strategy, where units behave in a linear fashion and the damage is concentrated in the relative weak masonry joints. Therefore, a composite interface model, formulated within the framework of plasticity, which includes tension cut-off for mode I failure, Coulomb friction envelope for mode II failure and cap mode for compressive failure was considered to model the nonlinear behaviour of the joints (Lourenço and Rots 1997). Due to the low dilatancy exhibited by masonry joints, the model was formulated in the context of non-associated plasticity.

The semicircular masonry arches had a 750 mm radius, 450 mm width and 50 mm ring thickness. The displacements at the abutments were restrained in both orthogonal directions, see Figure 1a. The complete setup description can be found in Oliveira et al. (2006) and Basilio (2007). Numerical analyses were performed with a finite element program including discontinuities by means of interfaces. The two dimensional mesh adopted in the analysis includes eight-noded plane stress elements to represent the masonry units, six-noded interface elements to simulate the mortar and GFRP-masonry joints and three-noded beam elements to represent the GFRP, see Figure 1b. Each masonry unit was modelled with four elements. In this case zero thickness interfaces were assumed for all the joints. Most of the properties used to simulate the mortar and GFRP-masonry interfaces were characterized within the experimental work, otherwise were obtained from mean values of previous works, see also Valluzzi et al. (2001) and Lourenço and Martins (2001).

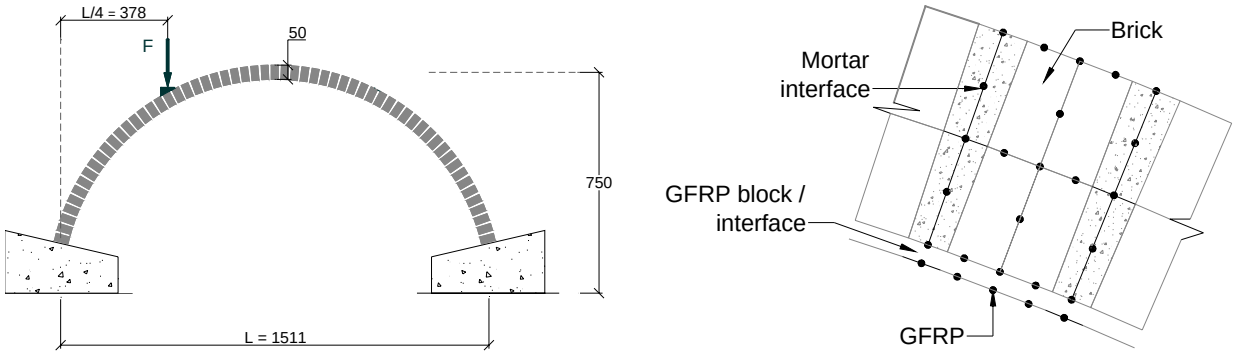

(a) (b)

Figure 1. Modelling of semicircular arches: (a) Elevation view (in mm); (b) Mesh detail of the masonry arch and GFRP strip.

Here, the following values were adopted: i) for masonry, a Young's modulus of 5000 N/mm^2; for the masonry joints, a tensile strength of 0.18 N/mm^2 and a shear strength of 0.3 N/mm^2; ii) for the composite, a shear bond strength of 0.65 N/mm^2, a tensile bond strength of 0.44 N/mm^2, a Young's modulus of 80000 N/mm^2 and a tensile strength of 3430 N/mm^2. Other values adopted in this paper include: for all joints, tangent of the internal friction angle of about 0.75 and zero dilatancy. The softening properties were estimated.

UNSTRENGTHENED ARCHES

In order to identify the structural behaviour, the maximum load capacity and the mechanism of collapse, an analysis of plain arches was carried out. This analysis gave a general overview about how the structure behaved under an increasing load applied at the quarter span, without any strengthening. The deformed shape provided an indication on its behaviour, showing where subsequent arches should be reinforced, especially in the case of localized strengthening. The numerical model shows a reasonable agreement with the experiments in the sense that it reproduces the initial stiffness and peak load, as illustrated in Figure 2. As observed experimentally, a sudden drop in the load carrying capacity after reaching the peak load was obtained. Failure was characterized by brittle behaviour, as depicted in Figure 2a. For a better perception of the structural behaviour, hinges appearance sequence is shown on the numerical load-displacement curve outlined in Figure 2b.

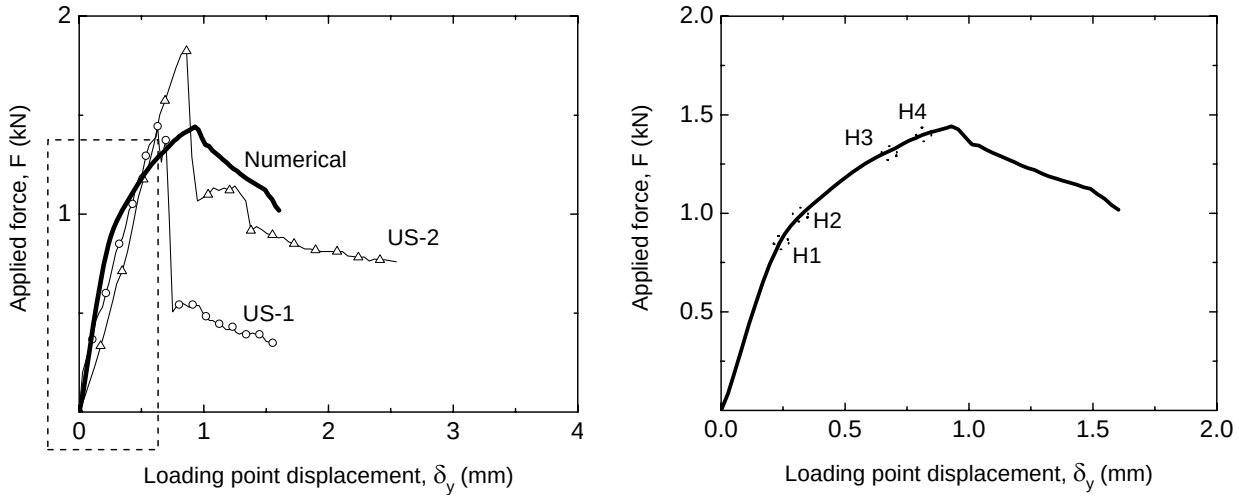

Figure 2. Unstrengthened arches: (a) experimental US-1 and US-2 results compared with its corresponding numerical response; (b) indication of plastic hinges sequence on the load-displacement diagram

Along with the deformed arch shape, also the principal compressive stresses are included in Figure 3 (all values presented are in kN/m^2). Each frame of Figure 3 has a filled dot indicating the current hinge developed, where the unfilled circle represents a hinge previously developed. Each hinge, marked with an intermittent circle, results in slight stiffness changes along the structural response path. All four hinges were formed before the peak load was reached and were detected at their very beginning development.

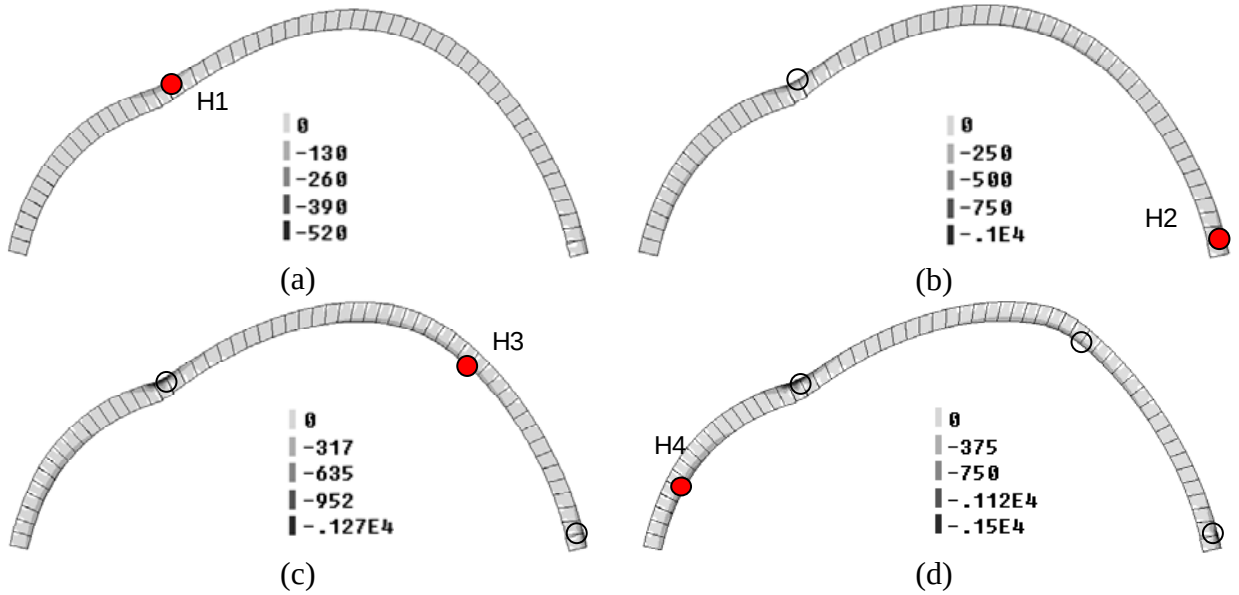

Figure 3. Numerical sequence of hinges formation for the unstrengthened masonry arch, including principal compressive stresses (kN/m^2) depicted on the incremental deformed mesh.

In order to provide a comparison between experimental and numerical results, as well as to make available a general overview about the various strengthening arrangements, Table 1 summarizes the quantitative data regarding the load capacity of each specimen, considering both experimental and numerical results.

Table 1. Maximum load sustained by arches.

Specimen	Maximum load P_{max} (kN)			Differences (%)
	Experimental		Numerical	
	Individual specimen	Average		
US-1	1.43	1.68	1.53	9
US-2	1.92			
LS-1	3.18	2.96	2.07	30
LS-2	2.73			
CSE-1	2.51	3.17	3.01	5
CSE-2	3.82			
CSE-3	3.62	3.44	3.50	2
CSE-4	3.26			
CSI-1	4.26	4.45	3.93	12
CSI-2	4.63			

LOCALLY STRENGTHENED ARCHES

Based on the collapse pattern observed for the two unstrengthened arches, originating four plastic hinges, and since both arches did not fall down at the end of the test, it was decided to reinforce them. With the exception of the foot hinge, a localized reinforcement was place at the extrados or at the intrados, where the three hinges were formed. Three partial length strips were placed on the semicircular perimeter of the arch. The configuration adopted was prepared in such a way that a GFRP strengthening of 160 mm width (two strips of 80 mm width each) was placed at the intrados or at the extrados, over each plastic hinge. Both the experimental and the numerical responses considering this partial length reinforcement are illustrated in Figure 4.

Because the analysis was carried out using a previous damaged arch, the numerical response reflects differences on stiffness and peak load, when compared with the experimental series, see Table 1. The mechanism of collapse shows that the location of the hinges moves towards the zone where reinforcement was absent. Smaller opening of hinges was developed, which might be attributed to less damage in the strengthened structure. The numerical failure pattern, with sliding between brick and mortar in the first joint, close to the springer, is similar to failure mechanisms reported by Creazza et al. (2002).

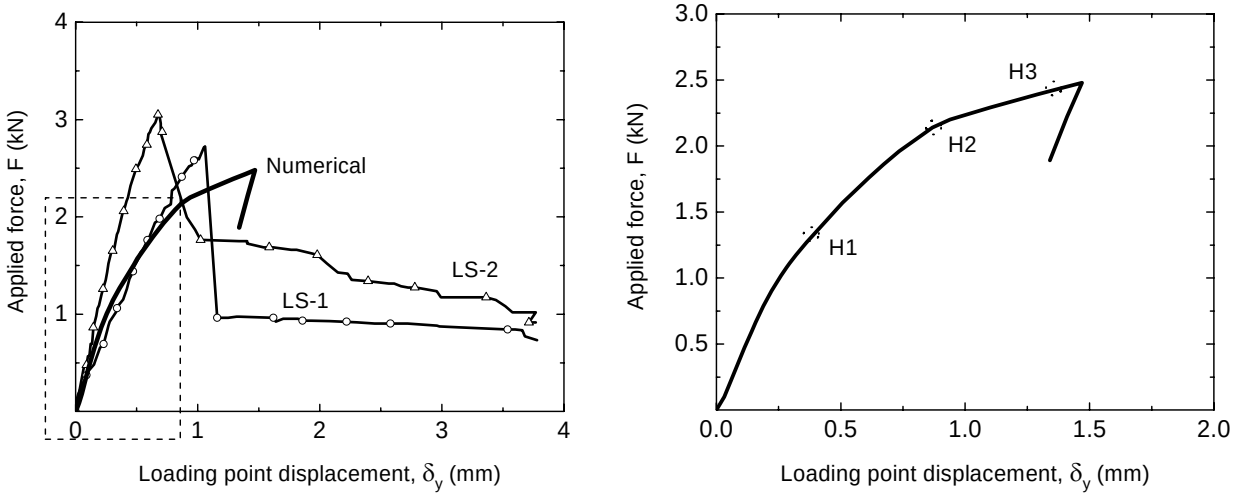

(a) (b)

Figure 4. Locally strengthened arches: (a) experimental LS-1 and LS-2 results compared with its corresponding numerical response; (b) representation of plastic hinges on the load-displacement diagram.

The localized reinforcement changed the mechanism of collapse of the unstrengthened arch, with a new location for the plastic hinges. Hinges appearance and sequence are illustrated over the incremental deformed mesh in Figure 5. The mesh includes also the principal compressive stresses corresponding to each plastic hinge formation. The numerical hinges detected for the localized strengthening option show more abrupt stiffness changes than plain arches.

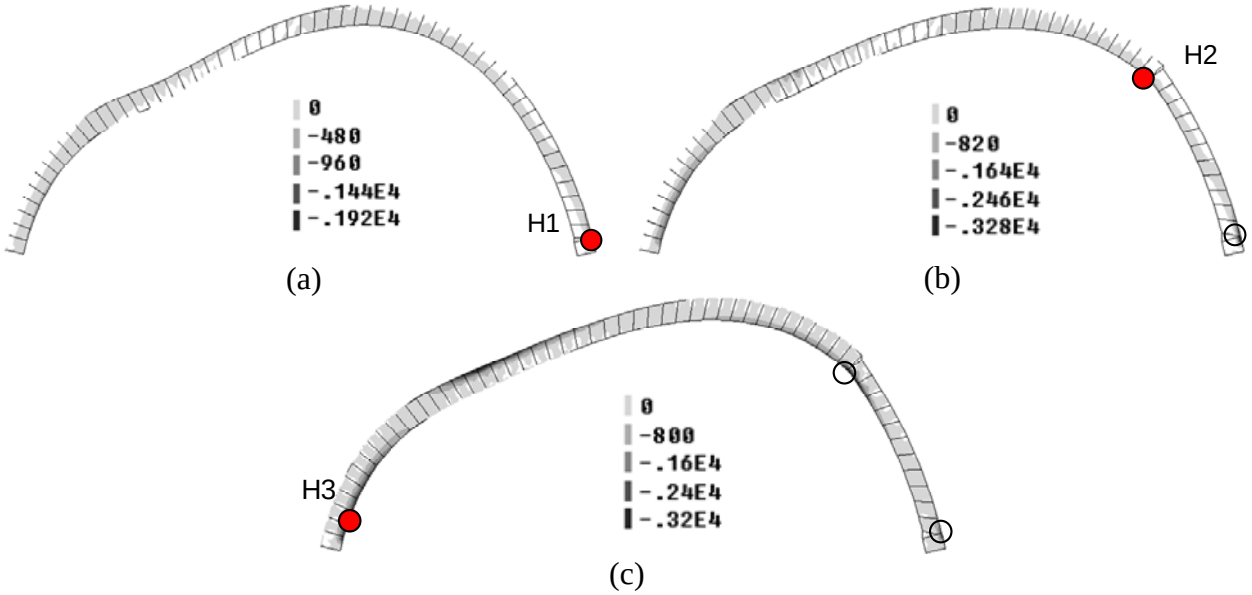

(a) (b)

(c)

Figure 5. Numerical sequence of hinge formation for the locally strengthened masonry arches, including principal compressive stresses (kN/m^2) depicted on the incremental deformed mesh.

CONTINUOUSLY STRENGTHENED ARCHES AT THE EXTRADOS

For the arches strengthened with continuous strips, a different collapse mechanism was expected since the presence of the fibres along the extrados or intrados prevents the fourth plastic hinge from occur. For the continuous strengthened specimens at extrados (CSE-1 and CSE-2), the first hinge was formed underneath the load point, whereas the other two hinges appeared at the supports. The collapse of the arch was due to sliding at the abutments.

Numerical results related to the full length reinforcement at the extrados are shown in Figure 6 and Figure 7. For this strengthening strategy, higher peak loads were reached, when comparing with plain arches and partial length reinforcement, as shown in Table 1. The initial stiffness is well captured, as shown in Figure 6a. The numerical result shows a premature failure, not observed in experiments. Therefore, it became unfeasible to capture the experimental ductility. No second order effects were considered in the numerical analysis.

The formation of the three hinges was clearly detected at successive stages, see Figure 7. The fourth hinge was prevented from occur and the mechanism of collapse was due to sliding of the foot arch, opposite to the loading point.

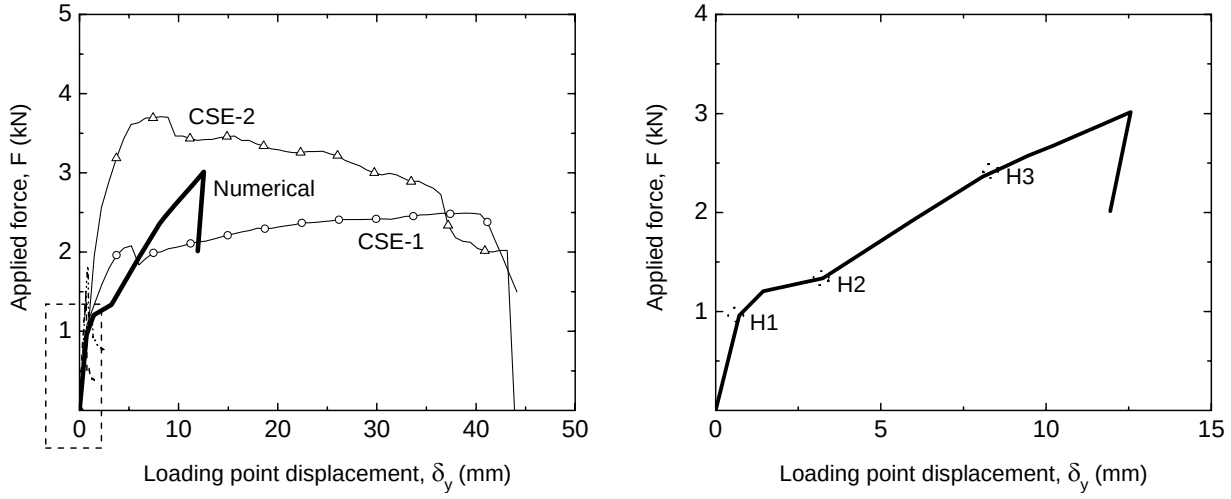

Figure 6. Continuously strengthened arches at the extrados: (a) experimental CSE-1 and CSE-2 results compared with its corresponding numerical response; (b) representation of the plastic hinges appearance on the load-displacement diagram.

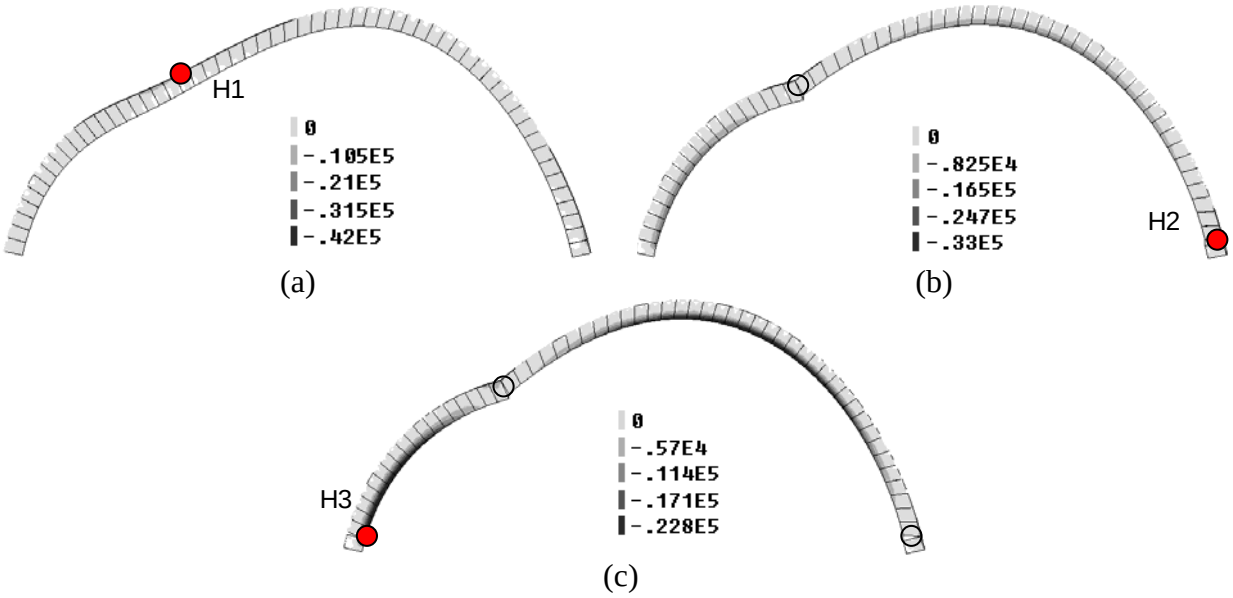

Figure 7. Numerical sequence of hinge development for the CSE arch, including principal compressive stresses (kN/m^2) depicted on the incremental deformed mesh.

CONTINUOUSLY STRENGTHENED ARCHES AT THE INTRADOS

For the continuous strengthened specimens at intrados (CSI-1 and CSI-2), two of the three hinges were formed at the supports, whereas the third one appeared on the less-load half of the arch. The fibres were able to maintain equilibrium until total collapse of the specimens. Failure occurred by sliding of the foot arch with FRP detachment.

Figure 8a compares both the numerical and experimental responses for the continuous length reinforcement option at the intrados. Numerical analyses show that this type of arch presents higher peak load values, when compared with continuous length GFRP reinforcement placed at the extrados, see Table 1. For the reinforcement placed at the intrados, the load smoothly increases at a lower rate. In general terms, the numerical result for the continuous strengthening at the intrados shown in Figure 8a can be considered a good approach to experiments, in terms of maximum load and deformability.

Figure 8b presents the hinges detected in the numerical response of the CSI arch and represented along the load-displacement diagram, as shown before for the other arches. The hinges detected mark perceptible stiffness changes, as happened with some of the previous numerical results presented, compare Figure 8b with Figure 6b.

For both intrados and extrados continuous strengthening, the last two plastic hinges appeared approximately in the same section, whereas the first hinge location was fully conditioned by the strengthening strategy, see Figure 7 and Figure 9.

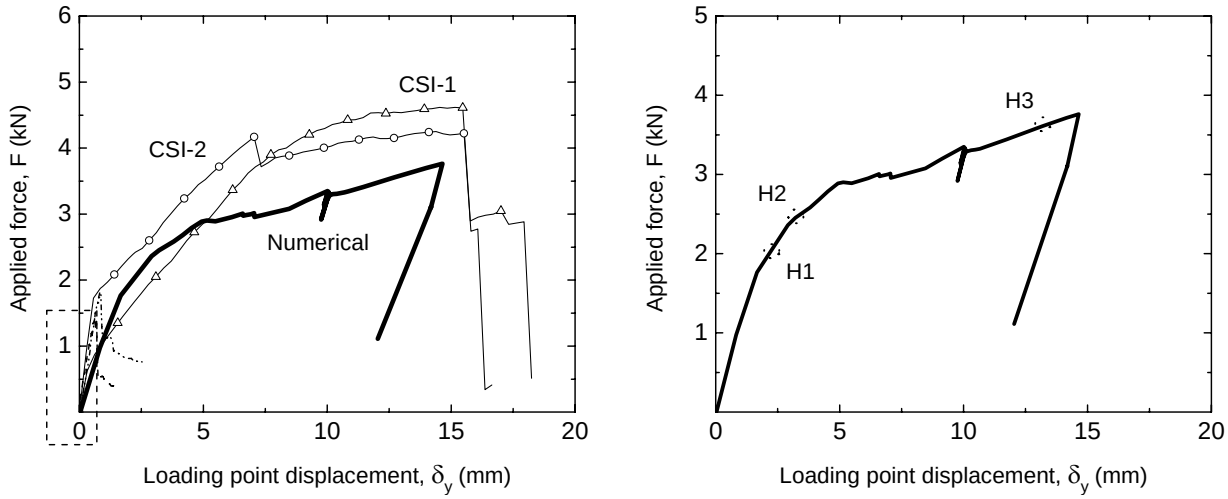

(a) (b)

Figure 8. Continuously strengthened arches at the intrados: (a) experimental CSI-1 and CSI-2 results compared with its corresponding numerical response; (b) representation of plastic hinges on the load-displacement diagram.

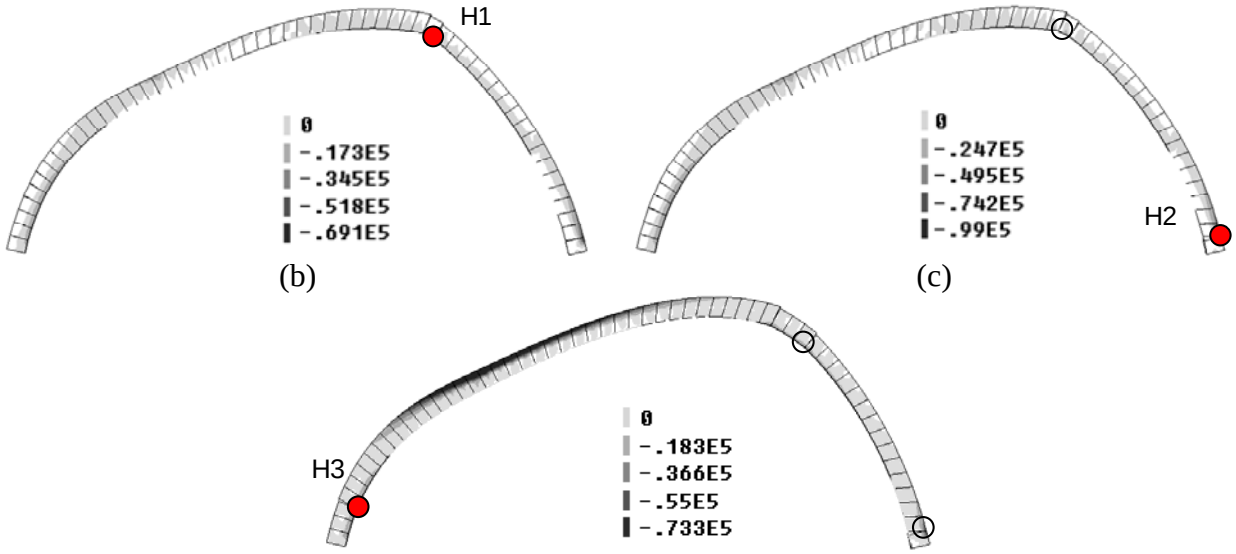

Figure 9. Hinge development sequence for the numerical CSI arch, including principal compressive stresses (kN/m^2) depicted on the incremental deformed mesh.

For the continuous strengthening at the intrados surface, after the development of the three hinges, the mechanism of failure was composed by the detachment of the FRP strip from the inner surface. Such fact is represented by a zoom at the loaded point, illustrated in Figure 10. Together with the experimental load-displacement curve beneath the loaded point, the initial stiffness and the mechanism of failure were captured by the numerical model.

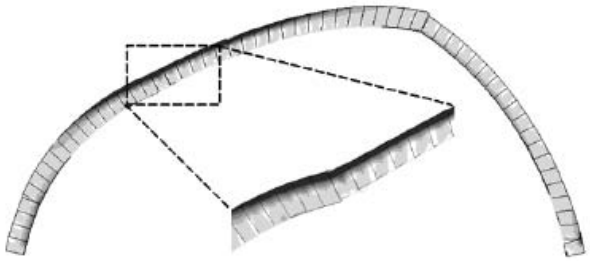

Figure 10. Detachment of the GFRP strip beneath the loaded point, represented on the deformed mesh.

SUMMARIZED CONCLUSIONS

This paper presents a plane stress finite element model developed to reproduce experimental results concerning semi-circular masonry arches strengthened with composite materials. The details of the modelling have been explained and discussed. The finite element model allowed a better understanding of the FRP-strengthening effects. With this model, it was possible to obtain similar peak loads and mechanisms of failure. However, the model did not succeed to reproduce all the experimental load-displacement curves observed. Probably this fact was due to the absence of an adequate constitutive model for the FRP-masonry interface, which is not available. Authors are currently working on the development of such constitutive law.

The application of FRP, as a reinforcement of plain arches, changed the four hinge failure mechanism. Instead, the arches strengthened continuously develop only three hinges and one additional "release". The detachment of the FRP, for the case where the strengthening was applied at the intrados, was captured by the numerical modelling.

ACKNOWLEDGEMENTS

This work was sponsored by the Portuguese Science and Technology Foundation (FCT), contract POCTI-ECM-38071-2001 "Strengthening of masonry arches with composite materials". The first author is grateful to the CONACYT for the scholarship granted.

REFERENCES

Basilio, I. "Strengthening of arched masonry structures with composites materials", *PhD Dissertation*, Universidade do Minho, Guimarães, Portugal, 2007, pp. 250.

Creazza, G., Matteazi R., Ana S., and Vitaliani R., "Analyses of masonry vaults: A macro approach based on three-dimensional damage model" *Journal Structural Engineering*, Vol. 128, No. 5, 2002, pp. 646–654.

Lourenço, P.B. and Rots J.G., "A multi-surface interface model for the analysis of masonry

structures", *Journal Engineering Mechanics*, Vol. 123, No. 7, 1997, pp. 660–668.

Lourenço, P.B. and Martins J.P., "Strengthening of the architectural heritage with composite materials", *In Proc. Composites in Constructions*, Figueiras et al (eds), Swets and Zeitlinger, 2001, pp. 571–576.

Oliveira, D.V., Basilio, I. and Lourenço, P.B., "FRP strengthening of masonry arches towards an enhanced behaviour", IABMAS'06, 2006, pp. 9.

Valluzzi, M.R., Valdemarca M., and Modena C., "Behaviour of brick masonry vaults strengthened by FRP laminates" *ASCE Journal of Composites for Construction*, Vol. 5, No. 5, 2001, pp. 163–169.